Acta Astronautica 139 (2017) 34–41

Contents lists available at ScienceDirect

Acta Astronautica

journal homepage: www.elsevier.com/locate/actaastro

Analysis of the effect of attachment point bias during large space debris removal using a tethered space tug

Zhongyi Chu [a,*], Jingnan Di [a], Jing Cui [b]

[a] School of Instrumental Science and Opto-electronics Engineering, Beihang University, 100191, China
[b] School of Mechanical Engineering and Applied Electronics, Beijing University of Technology, 101100, China

ARTICLE INFO

Keywords:
Space debris removal
Space tethered system
Attachment point bias
Effect analysis

ABSTRACT

Space debris occupies a valuable orbital resource and is an inevitable and urgent problem, especially for large space debris because of its high risk and the possible crippling effects of a collision. Space debris has attracted much attention in recent years. A tethered system used in an active debris removal scenario is a promising method to de-orbit large debris in a safe manner. In a tethered system, the flexibility of the tether used in debris removal can possibly induce tangling, which is dangerous and should be avoided. In particular, attachment point bias due to capture error can significantly affect the motion of debris relative to the tether and increase the tangling risk. Hence, in this paper, the effect of attachment point bias on the tethered system is studied based on a dynamic model established based on a Newtonian approach. Next, a safety metric of avoiding a tangle when a tether is tensioned with attachment point bias is designed to analyse the tangling risk of the tethered system. Finally, several numerical cases are established and simulated to validate the effects of attachment point bias on a space tethered system.

1. Introduction

With the increasing level of human activities in space, the problem of space debris occupying valuable orbital resource is inevitable. Despite the enactment of debris mitigation measures and improved cognition of orbiting space debris, the ability to scavenge large space debris located along the operating orbit is still a major issue [1]. Large debris (spent rocket stages, defunct satellites, etc.) is more prone to collisions, which can produce tens of thousands of pieces of new debris [2]. Therefore, it is urgent to safely clear large abandoned targets to ensure the safety of spacecraft operating in orbit [3].

The use of a tether for debris removal has been proposed [4] with the advantages of wider operating ranges and low costs. Many scholars have presented in-depth studies regarding the application of tethers; such studies mainly include the two categories of momentum exchange tethers and electrodynamic tethers [5]. The concept of active debris removal (ADR) has been proposed to safely remove high-risk debris, such as large massive debris [6–8], aiming to de-orbit the predetermined debris captured by a dedicated tethered spacecraft via active thrust. A notable project called ROGER (Robotic Geostationary Orbit Restorer) was developed by the ESA (European Space Agency) [9,10] to capture and de-orbit a redundant GEO (geostationary orbit) satellite using a tethered net or mechanical claw. Specifically, once the debris is captured by a manipulator, such as a harpoon, a mechanical hand or a net, a tethered spacecraft system (TSS) is established to achieve de-orbiting of a passive, non-cooperative, possibly spinning target.

However, the flexibility of the tether leads to several technical challenges regarding the stability of the TTS and increases the difficulty in control system design. In recent years, some researchers have studied the stability of the de-orbit system and improved some novel control approaches [11–19]. Nevertheless, especially for large spinning debris, the angular momentum of debris can also have a strong effect on active spacecraft, which may induce twining of the tether and even result in the loss of control of the system. Therefore, some achievements in dynamic analysis of the attitude of large debris have recently been proposed [20–23]. In Ref. [20], a simplified model of a tethered system is set using the Lagrange formalism to prove that the properties of the tether can affect the oscillation of the passive satellite. In addition, the slackness of the tether is of high risk of inducing tether tangling. Subsequently, flexible appendages are further taken into consideration in Ref. [21]; the choice of the stiffness of the tether was found to be important to avoid resonance between the tether and debris. Based on early work [20], Aslanov and Yudintsev [22] modelled the system using the Newtonian approach to further study additional effects, such as the thrust level,

* Corresponding author.
E-mail address: chuzystar@gmail.com (Z. Chu).

http://dx.doi.org/10.1016/j.actaastro.2017.06.028
Received 2 February 2017; Received in revised form 2 June 2017; Accepted 27 June 2017
Available online 28 June 2017

orbital motion and atmospheric drag on system. In addition, the initial angle between the tether and vector from the mass of the debris to the attachment point is involved in the simulation case, which significantly affects the amplitude of the oscillation of passive debris. Moreover, several simulation cases are also studied in Ref. [23], which proposes a novel sub-tether structure to reduce the oscillation of the debris. Although the effect of many parameters mentioned above has been studied on a tethered system, attachment point bias is always neglected entirely to simplify the model or is simplified in the simulation with the variation of other parameters. In fact, attachment point bias can change the acting point and arm of tether tension on debris, which easily occur in actual operation during the capture phase. Therefore, attachment point bias can significantly influence the motion of the debris, even leading to a crippling tangle. However, the specific effects of the bias have hardly been studied, making it significant to study the effect of attachment point bias on the motion of debris with a tangling risk. Here, the novelty of the work is as follows. First, the effect of different biases of the attachment point on the motion of debris relative to the tether with the tangling risk is analysed. Next, the safety metric for avoiding a tangle when the tether is tensioned is designed to analyse the tangling risk of the system with attachment point bias. Finally, several simulation cases are implemented to validate the effect of attachment point bias with the safety metric.

This paper includes five main sections. In Section 2, the effect of attachment point bias on the motion of debris relative to the tether is analysed based on a dynamic model established using a Newtonian approach. Based on that model, in Section 3, the safety metric of avoiding a tangle when the tether is tensioned with attachment point bias is designed to analyse the tangling risk of the tethered system. Next, several numerical cases are implemented to analyse the variation of the relative motion between the debris and tether caused by different biases of the attachment point in the post-capture phase in Section 4. Finally, conclusions are summarized in Section 5.

2. Analysis of the effect of attachment point bias on the motion of debris relative to the tether

2.1. Assumptions and reference frames

As shown in Fig. 1, large space debris (non-cooperative, nonfunctional, passive objects) is regarded as a rigid body, hereafter referred to as a target, and the active space tug is considered to be a particle. A visco-elastic tether is used to connect the space tug to the target. In addition, the active de-orbit force of the system is provided by a rocket thruster on the space tug.

We focus on the attitude of large passive debris (hereinafter referred to as the target) relative to the tether. The mass of the visco-elastic tether is far less than the end bodies and can be neglected. In addition, bending of the tether is also ignored when the tether is tensioned because of its short length. Moreover, the short-time consumption of fuel is neglected as well.

Based on the assumptions mentioned above, the following reference frames (shown in Fig. 1) used in describing the system are introduced:

(1) The Earth centred inertial reference frame $\Re_I$, the origin of which coincides with Earth's centre O_e, $\vec{O_e x_e}$ points to the vernal equinox, $\vec{O_e z_e}$ is perpendicular to Earth's equatorial plane, and $\vec{O_e y_e}$ is determined afterwards using the right-hand rule.
(2) The local orbital coordinate frame $\Re_O$, its origin attached to the system centroid O, $\vec{O z_o}$ points to O_e, $\vec{O x_o}$ is perpendicular to $\vec{O z_o}$ in the orbital plane and lying behind the target, and is $\vec{O y_o}$ determined afterwards using the right-hand rule.
(3) The body fixed frame of target $\Re_T$, its origin coincides with the target centroid O_t, $\vec{O_t x_t}$, $\vec{O_t y_t}$ and $\vec{O_t z_t}$, which coincide with three principal inertial axes, respectively, conforming to the right-hand rule.

2.2. Analysis of the effect of the attachment point bias on a space tethered system

As shown in Fig. 1, the space tethered system consists of a space tug, a massless visco-elastic tether and a large passive target. The motion of the space tug and target is considered in $\Re_I$ with the following equations:

$$m_c \ddot{\boldsymbol{r}}_c = -\mu m_c \boldsymbol{r}_c / r_c^3 + \boldsymbol{F}_{th} - \boldsymbol{T} \tag{1}$$

$$m_t \ddot{\boldsymbol{r}}_t = -\mu m_t \boldsymbol{r}_t / r_t^3 + \boldsymbol{T} \tag{2}$$

where m_c and m_t are the masses of the space tug and target, respectively; $\boldsymbol{r}_c$ and $\boldsymbol{r}_t$ are the position of the space tug and the target in $\Re_I$ respectively; $\boldsymbol{F}_{th}$ is the thruster force on the space tug; and $\boldsymbol{T}$ is the tension vector along the tether from the attachment point pointing to the space tug.

Thus, the motion of the system centroid can be described as

$$\boldsymbol{r} = \eta_c \boldsymbol{r}_c + \eta_t \boldsymbol{r}_t \tag{3}$$

$$\dot{\boldsymbol{r}} = \eta_c \dot{\boldsymbol{r}}_c + \eta_t \dot{\boldsymbol{r}}_t \tag{4}$$

where $\boldsymbol{r}$ and $\dot{\boldsymbol{r}}$ are the position and velocity of the system centroid and $\eta_c = m_c/m$, $\eta_t = m_t/m$ and m are the total mass of the system, i.e. $m = m_c + m_t$.

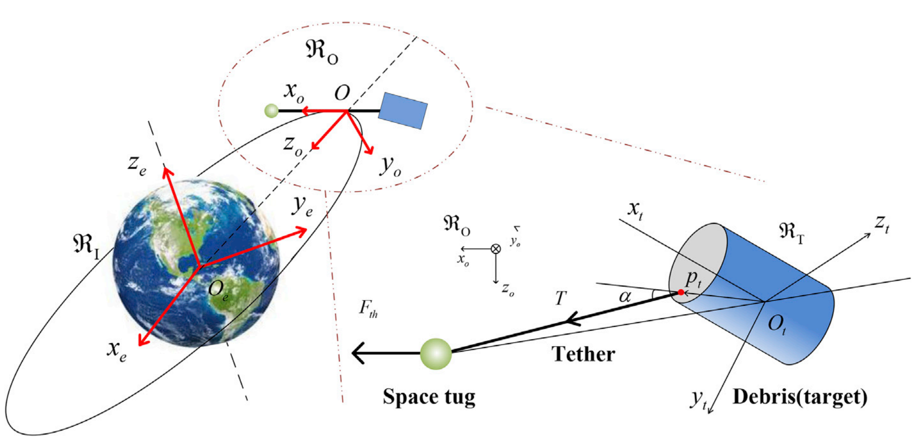

Fig. 1. Space tethered system in active debris removal.

Thus, the rotation matrix transforming the coordinates from $\Re_I$ to $\Re_O$ is obtained by

$$C_i^o = [\boldsymbol{i}, \boldsymbol{j}, \boldsymbol{k}]^{\mathrm{T}} \tag{5}$$

where

$$\begin{aligned} \boldsymbol{k} &= -\boldsymbol{r}/r \\ \boldsymbol{j} &= \boldsymbol{k} \times (\dot{\boldsymbol{r}}/|\dot{\boldsymbol{r}}|) \\ \boldsymbol{i} &= \boldsymbol{j} \times \boldsymbol{k} \end{aligned} \tag{6}$$

2.3. Based on the euler dynamics equation, there are

$$I_t\dot{\boldsymbol{\omega}}_t + \boldsymbol{\omega}_t \times I_t\boldsymbol{\omega}_t = \boldsymbol{M}_t = p_t \times \boldsymbol{T}^t \tag{7}$$

where $I_t = diag(I_{xx}, I_{yy}, I_{zz})$ and $\boldsymbol{\omega}_t$ are the inertia matrix and the angular velocity of the target represented in $\Re_T$, respectively. In addition, the torque $\boldsymbol{M}_t$ is obtained by the vector p_t (shown in Fig. 1) and tension force $\boldsymbol{T}^t$ in $\Re_T$.

Then, to avoid the numerical singularity, the quaternion $\boldsymbol{Q}_t = [q_{t0}, q_{t1}, q_{t2}, q_{t3}]^{\mathrm{T}}$ is used to represent the attitude of the target and is solved by

$$\dot{q}_{t0} = -\frac{1}{2}\boldsymbol{q}_t^T\boldsymbol{\omega}_t \tag{8}$$

$$\dot{\boldsymbol{q}}_t = \frac{1}{2}\left(q_{t0}E_{3\times3} + \boldsymbol{q}_t^{\times}\right)\boldsymbol{\omega}_t \tag{9}$$

where $E_{3\times3} = diag(1,1,1)$, $\boldsymbol{q}_t = [q_{t1}, q_{t2}, q_{t3}]^{\mathrm{T}}$, and $\boldsymbol{q}_t^{\times}$ is a tensor according to

$$\boldsymbol{q}_t^{\times} = \begin{pmatrix} 0 & -q_{t3} & q_{t2} \\ q_{t3} & 0 & -q_{t1} \\ -q_{t2} & q_{t1} & 0 \end{pmatrix} \tag{10}$$

Thus, the rotation matrix transforming the coordinates from $\Re_O$ to $\Re_T$ can be solved by

$$C_o^t = \left(q_{t0}^2 - \boldsymbol{q}_t^T\cdot\boldsymbol{q}_t\right)\cdot E_{3\times3} + 2\left(\boldsymbol{q}_t\cdot\boldsymbol{q}_t^T\right) - 2q_{t0}\cdot\left[\boldsymbol{q}_t^{\times}\right] \tag{11}$$

Therefore, the rotation matrix transforming the coordinates from $\Re_I$ to $\Re_T$ can also be obtained as

$$C_i^t = C_i^o\cdot C_o^t \tag{12}$$

and the rotation matrix from $\Re_T$ to $\Re_I$ is $C_t^i = [C_i^t]^{\mathrm{T}}$.

2.4. Naturally, there is

$$\boldsymbol{T}^t = C_i^t\cdot\boldsymbol{T} \tag{13}$$

Subsequently, the tension force using a visco-elastic tether is determined by

$$\boldsymbol{T} = \varepsilon_{l_0}\left[k_t(l - l_0) + c_t\dot{l}\right]\cdot\boldsymbol{e}_l \tag{14}$$

where

$$\varepsilon_{l_0} = \begin{cases} 1 & l > l_0 \\ 0 & l \le l_0 \end{cases} \tag{15}$$

$$\boldsymbol{e}_l = \frac{1}{l}\left(\boldsymbol{r}_c - \boldsymbol{r}_t - C_t^i\boldsymbol{p}_t\right) \tag{16}$$

In addition, k_t and c_t are the stiffness and damping of the tether, respectively. l and l_0 are the actual length and natural length, respectively. $\boldsymbol{e}_l$ is a unit vector in $\Re_I$ along the tether from the attachment point pointing to the space tug.

To analyse the tangling risk of the tethered system, the angle α is used to describe the relative attitude between the tether and target in the following study and is defined as the angle between the vector $\boldsymbol{p}_t$ and $\boldsymbol{T}$, as shown in Fig. 1. Thus, there is

$$\alpha = arccos\left(\frac{\boldsymbol{p}_t^T\boldsymbol{T}^t}{|\boldsymbol{p}_t||\boldsymbol{T}^t|}\right) \tag{17}$$

where $\frac{\boldsymbol{T}^t}{|\boldsymbol{T}^t|} = \boldsymbol{e}_l^t = C_i^t\boldsymbol{e}_l$, which can be obtained from Eq. (12) and Eq. (16). Thus, the Eq. (17) can be rewritten as

$$\alpha = arccos\left(\frac{\boldsymbol{p}_t^T\boldsymbol{e}_l^t}{|\boldsymbol{p}_t|}\right) \tag{18}$$

As shown in Fig. 1, tangling is more dangerous when angle α is a larger value. Thus, angle α is a reasonable parameter to analyse the tangling risk of a system.

From Eq. (18), it is obvious that the attachment point bias is an immediate and significant factor that affects the motion of debris relative to the tether. Therefore, it is necessary to study the dynamic effect on a tethered system caused by attachment point bias.

3. Safety metric of avoiding tangle

Once the target is captured by a manipulator, such as a harpoon or mechanical hand, a tug-tether-target combination is established and a maximum of angle α without tangling, i.e. α_s, exists when the tether is tensioned. In other words, when

$$\alpha < \alpha_s \tag{19}$$

the tensioned tether is not tangled.

Generally, if and only if there is no bending caused by the contact between the tether and target, except for the attachment point, the tethered system can avoid the occurrence of tangling. A critical limit must exist between tangling and no-tangling, where a tether just comes into contact with the surface target with no bending. Thus, there is a cluster of angle α, i.e. $\{\alpha_i\}, i = 1, 2, 3, \cdots$, to describe the limit mentioned above, satisfying that two or more contact points exist between tether and surface of target. It is obvious that when

$$\alpha < \alpha_i, i = 1, 2, 3, \cdots \tag{20}$$

A tangle does not occur with a tensioned tether. In addition, the value of α_i can be determined based on the position of the capture and geometry of target in different cases.

Thus, according to Eq. (19) and Eq. (20), α_s can be determined by

$$\alpha_s = \min(\{\alpha_i\}) \tag{21}$$

For example, in the post-capture phase, there are two typical circumstances that occur, 1) the attachment point is located in the main body, as shown in Fig. 2(a1) and Fig. 2(a2), or 2) the target is gripped on the appendages, as shown in Fig. 2(b1) and Fig. 2(b2). Therefore, two types of α_s are determined by the method mentioned above corresponding to these two circumstances.

As Fig. 2(a2) shows, when the attachment point is located in the main body, a tangle can only occur in the edge of the main body. To determine the value of α_s, the mentioned $\{\alpha_i\}$ should be determined. First, the angle $\theta_i \in [0, \pi]$ is used to describe different directions of the tether corresponding to α_i as

$$\theta_i = \langle \boldsymbol{e}_p, \boldsymbol{T}_i \rangle \tag{22}$$

where $< \boldsymbol{e}_p, \boldsymbol{T}_i >$ denotes the angle between the vector $\boldsymbol{e}_p$ and $\boldsymbol{T}_i$, and $\boldsymbol{e}_p$ is the unit vector from O_s pointing to attachment point P. When $\theta_i = 0$ or $\theta_i = \pi$, according to relation of the plane angle,

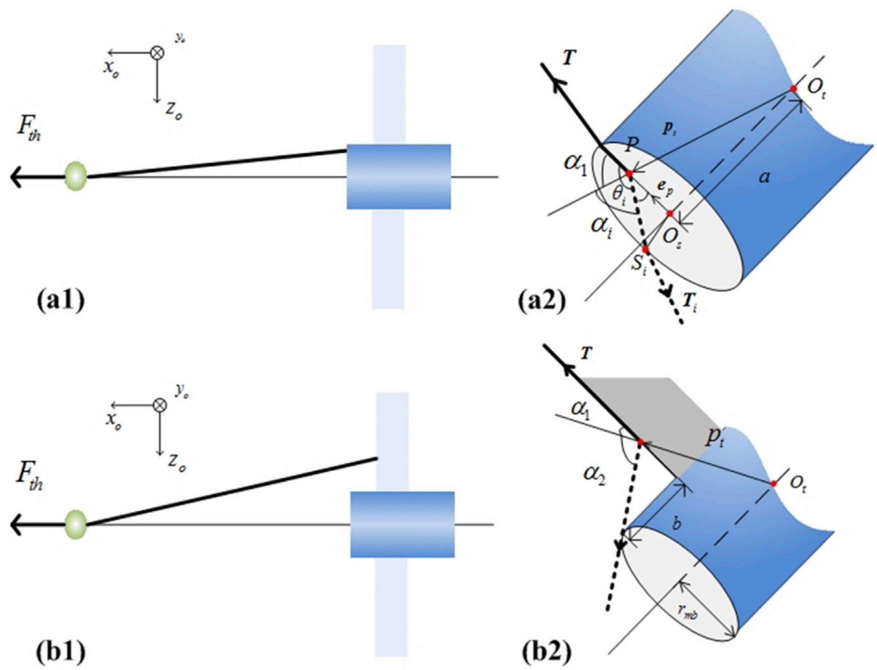

Fig. 2. Different initial capture position.

$$\alpha_1 = \frac{\pi}{2} - \langle \boldsymbol{p}_t, \overrightarrow{O_tO_s} \rangle \qquad \theta_1 = 0 \tag{23}$$

$$\alpha_2 = \pi - \alpha_1 \qquad \theta_2 = \pi \tag{24}$$

When $\theta_i \neq 0$ and $\theta_i \neq \pi$, a special tetrahedron is set by the point O_tO_sP and S_i shown in Fig. 2(a2), in which S_i is the tangle point in the edge of main body. Thus, the value of angle α_i, $i = 3, 4, \cdots$ is obtained by

$$\alpha_i = \pi - \angle O_tPS_i \tag{25}$$

where according to the 3-dimensional cosine theorems [24], there is

$$\cos\angle O_tPS_i = \cos\angle O_tPO_s \cdot \cos\angle O_sPS_i = \cos(\alpha_1)\cos(\pi - \theta_i) \tag{26}$$

Next, synthesizing Eq. (23), Eq. (24), Eq. (25) and Eq. (26), we obtain the value of $\{\alpha_i\}$ as

$$\alpha_i = \pi - \arccos[\cos(\alpha_1)\cos(\pi - \theta_i)] \qquad i = 1, 2, 3, \cdots \tag{27}$$

On the basis of and Eq. (21) and Eq. (27), the value of α_s can be calculated as

$$\alpha_s = \min(\{\alpha_i\}) = \alpha_1 \tag{28}$$

Similarly, when the attachment point is located in the appendages, as shown in Fig. 2(b2), there is

$$\alpha_s = \min(\alpha_1, \alpha_2) \tag{29}$$

where

$$\alpha_1 = \langle \boldsymbol{p}_t, \mathbf{e}_{ap} \rangle \tag{30}$$

$$\alpha_2 = \pi - \alpha_1 - \arctan\left(\frac{b}{\boldsymbol{p}_t \cdot \boldsymbol{e}_{ap} - r_{mb}}\right) \tag{31}$$

where $\boldsymbol{e}_{ap}$ is the unit vector of the attachment edge of the appendage and r_{mb} is the size of cross-section of the target main body. In this case, we can see that there are some α_i that can be ignored in actual analysis because of their obviously larger value in this cluster of angles.

4. Numerical examples and analysis

Based on the model built in Section 2, several simulation cases have been established to explore the effects of attachment point bias on the attitude of the target on GEO. The specific parameters of the tethered system are shown in Table 1.

Here, from Case 1 to Case 4, we study the performance of the oscillation of the target under attachment point biases during de-orbit phase with constant de-orbit thrust force F_{th} , as shown in Fig. 3(a). Next, three different situations with the same initial angle in the post-capture phase caused by attachment point biases (situation 1, Fig. 3(a)) and misalignment of the relative position (situation 2, Fig. 3(b)) and attitude (situation 3, Fig. 3(c)) between the space tug and target are studied in Case 5 and Case 6 with different initial angular velocities.

4.1. Case 1

First, we consider that the vector $\boldsymbol{p}_t$ along the axis O_tx_t is set as $[2\ 0\ 0]^{\mathrm{T}}$ and the initial attitude of target is $[1\ 0\ 0\ 0]^{\mathrm{T}}$ with an initial angular velocity $\omega_0 = [0 \quad 0 \quad 0]^T$, $\omega_1 = [0.05 \quad 0 \quad 0]^T$ and $\omega_2 = [0.1 \quad 0 \quad 0]^T$ rad/s relatively. This case is an ideal situation; however, it is difficult to achieve in actual operation. Relevant parameters are represented in Table 1. The simulation results with different initial angular velocities are shown in Fig. 4.

4.2. Case 2

The situation that the attachment point P is located somewhere close

Table 1
Specific parameters of the tethered system.

Parameter	Value	Parameter	Value
m_c	1000 kg	k_t	33 GPa
m_t	3000 kg	c_t	10 Ns/m
I_{xx}	3000 kg m^2	l_0	200 m
I_{yy}	10000 kg m^2	a	2 m
I_{zz}	10000 kg m^2	b	1 m
r_{t0}	42164 km	r_{mb}	1 m
F_{th}	5 N		

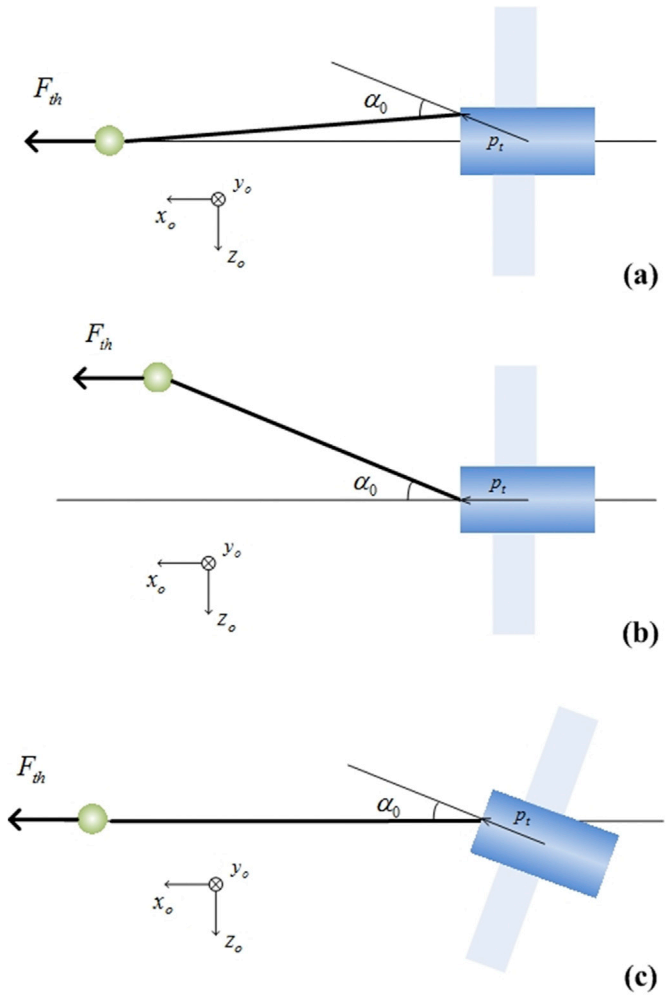

Fig. 3. Three different situations in the post-capture phase with the same initial angle.

to the edge of the main body is taken into account. Hence, vector $\boldsymbol{p}_t$ is set as $[2\ 0.8–0.8]^{\mathrm{T}}$ in this case. Other parameters and initial conditions of the system in this case have no difference with Case 1. The history of angle α is shown in Fig. 5.

4.3. Case 3

Here, we consider that the target is captured by an actuator on one side of appendages, for example, solar panels. In this circumstance, the vector $\boldsymbol{p}_t$ is set as $[10–2]^{\mathrm{T}}$. Other parameters and initial conditions are the same as those of Case 1. The results of the simulation are shown in Fig. 6.

4.4. Case 4

The greater attachment point bias is studied in this case, where the vector $\boldsymbol{p}_t$ is set to $[10–3]^{\mathrm{T}}$. Similarly, there is still no difference for the other parameters and initial conditions between this case and the previous cases. Fig. 7 shows the simulation results of this case.

To analyse the variation trend of angle α and safety of the tethered system with different attachment point biases, the maximum of angle α and safety value α_s from Case 1 to Case 4 are extracted and represented in Fig. 8. It can be seen that the maximum amplitude of oscillation is significantly enlarged with the increase of the attachment point bias. In addition, the safe range is also reduced with the increase of the bias. In other words, a higher risk of tangling exists when there is a greater bias of capture. Moreover, although the existence of initial angular momentum in Case 1 makes smaller oscillation due to gyroscopic inertia of large debris along the ideal axis, it can cause a greater and more complex oscillation when large attachment point bias exists. Meanwhile, the tangling risk becomes greater with the increase of initial angular velocity as shown in Fig. 8.

However, the initial value of angle α caused by an initial misalignment of the relative attitude between the tug and target also affects the variation of angle α in the course of ADR [16], which can be induced by attachment point bias as well. Thus, it is necessary to explore the substantial effects of attachment point bias on the system by comparison with other two situations (Fig. 3(b) and (c)) with the same initial value of angle α.

Previous cases have studied the effect of different attachment point biases on the system, which causes different initial angle α_0 as well. To determine the actual effect of the bias, three different situations caused by different misalignments in the post-capture phase with the same initial angle are studied in the following case 5 and case 6.

4.5. Case 5

In this case, the vector $\boldsymbol{p}_t$ and initial attitude $\boldsymbol{q}_0$ of three different situations mentioned with the same initial angle $\alpha_0 = 1.117$ rad are set in Table 2.

The initial angular velocity in this case is.

$$\omega_{t0} = [0.05 \quad 0 \quad 0]^T \cdot \mathrm{rad/s}$$

along axis $O_t x_t$ in three situations. The other parameters are the same as the above cases represented in Table 1. The specific behaviour of angle α is shown in Fig. 9.

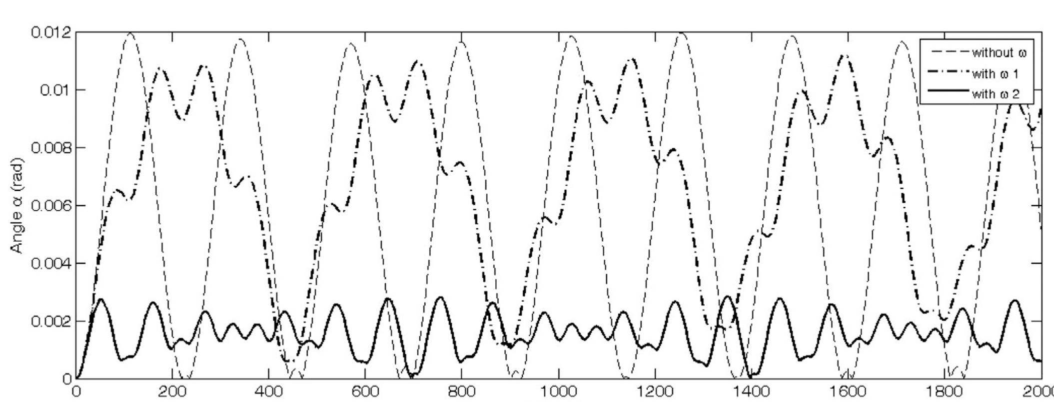

Fig. 4. The simulation result of angle α in Case 1.

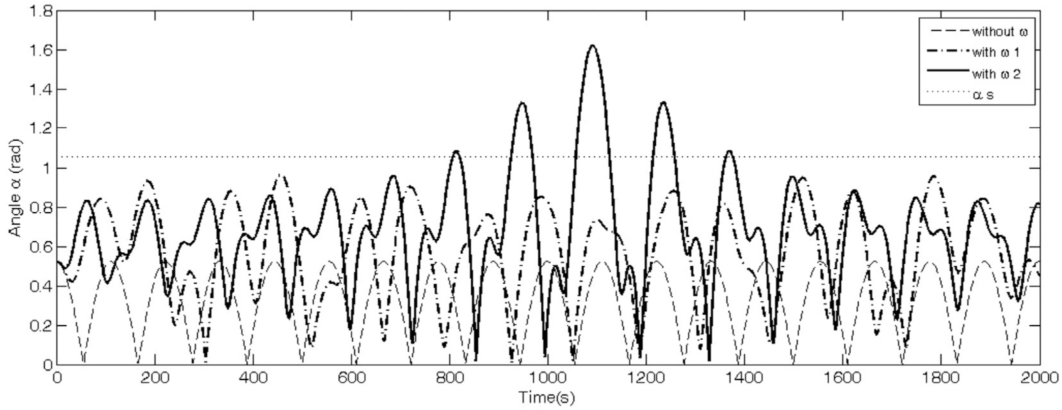

Fig. 5. The simulation result of angle α in Case 2.

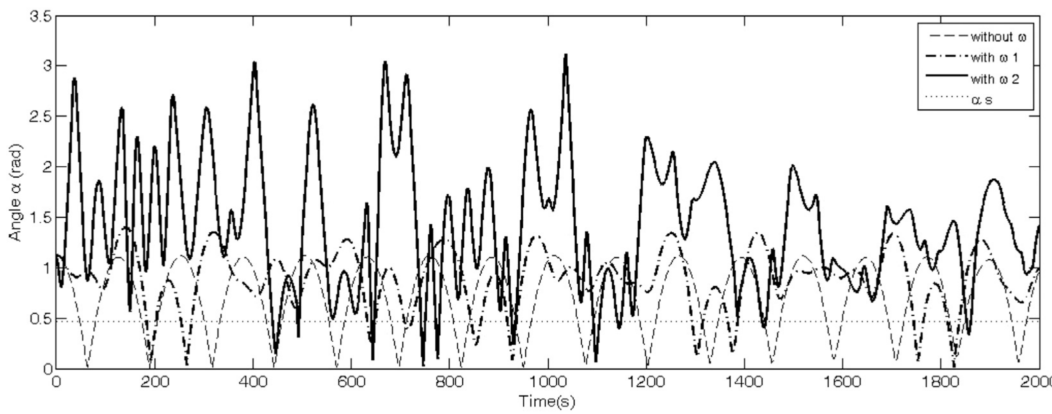

Fig. 6. The simulation result of angle α in Case 3.

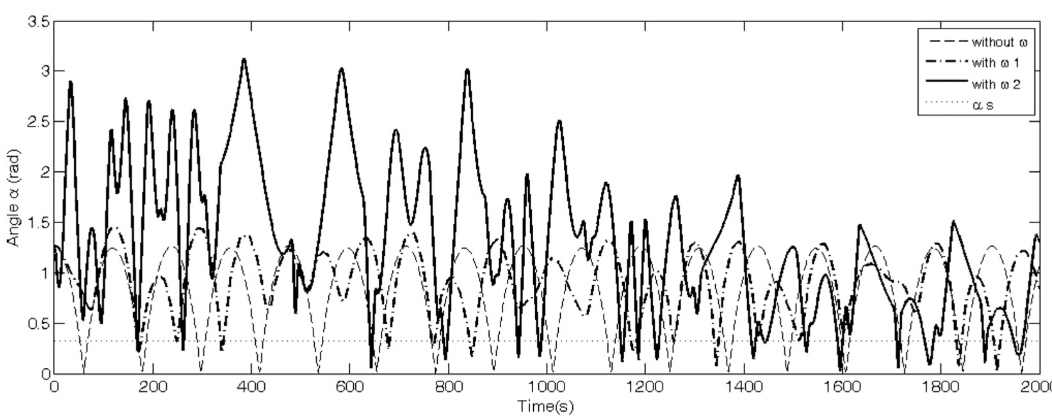

Fig. 7. The simulation result of angle α in Case 4.

4.6. *Case 6*

Finally, the behaviour of angle α is studied with different initial angular velocities as.

$$\omega_{t0} = [0.05 \quad 0.03 \quad 0.03]^T \cdot \text{rad/s}$$

under the same conditions of Case 5. The specific performance of angle α is shown in Fig. 10.

To analyse the actual effect of attachment point bias, the maximums of angle α of the three different situations mentioned above are extracted from Figs. 9 and 10 and are listed in Table 3.

As Table 3 shows, attachment point bias (situation 1) causes the greatest oscillation of the cases considered. In addition, the initial misalignment of the relative position between the space tug and target (situation 2) leads to more complicated motion of the target, which is coupled with a swing of the tug-tether-target combination. Moreover, the configuration with the attachment point bias exhibits extreme inability of the motion of target with angular rates in all three axes. In addition, compared with the other two situations, attachment point bias can more easily occur in actual operation because the operating distance between the space tug and target is much longer than the size of the target. In other words, the configuration with bias should be considered or avoided, which can be dangerous in de-orbiting missions of spinning

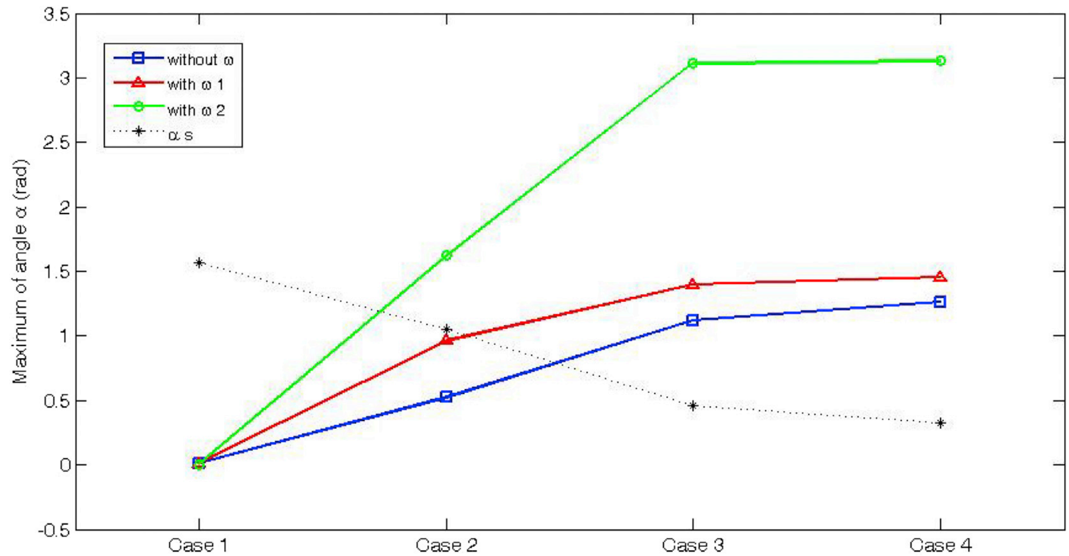

Fig. 8. Variation trend of angle α of Case 1 to Case 4.

large debris.

Table 2
Partial parameters in Case 5 and Case6.

Parameter	Situation 1	Situation 2	Situation 3
$\boldsymbol{p}_t$	$[1\ 0\ –2]^T$	$[2\ 0\ 0]^T$	$[2\ 0\ 0]^T$
$\boldsymbol{q}_0$	$[1\ 0\ 0\ 0]^T$	$[1\ 0\ 0\ 0]^T$	$[0.848\ 0\ 0.530\ 0]^T$

5. Conclusion

The use of a space tether is a promising means to perform large debris removal because of its wide operating ranges and low costs. However, the issue of tether tangling because of its flexibility presents a danger to the tethered system, the risk of which can be increased via attachment point bias. Hence, this paper analysed the effect of attachment point bias on the motion of debris relative to the tether in the post-capture phase based on

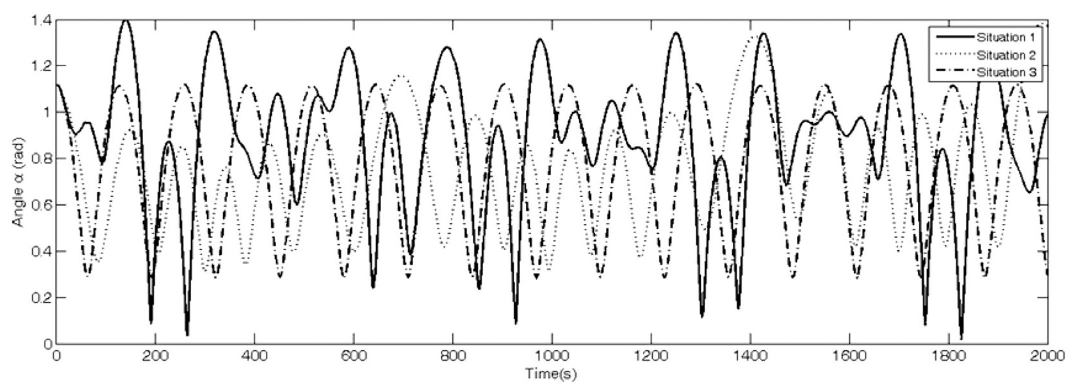

Fig. 9. The simulation result of angle α in Case 5.

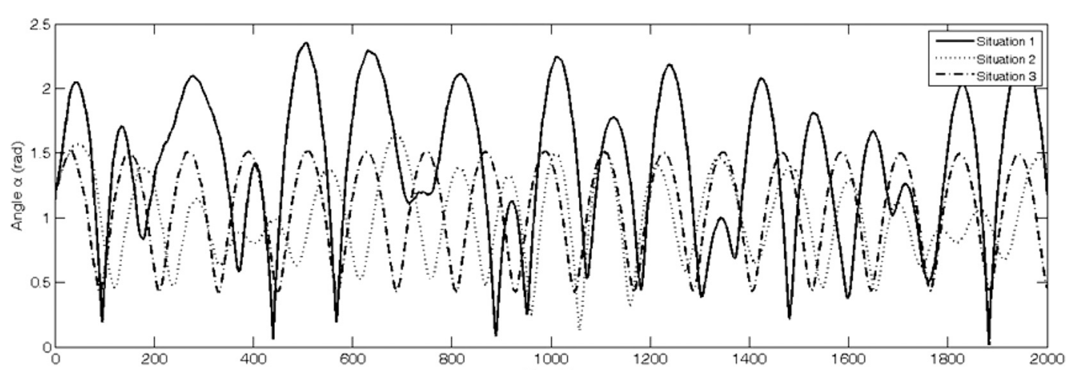

Fig. 10. The simulation result of angle α in Case 6.

Table 3
Maximums of angle α in case 5 and case 6.

Cases	Maximum of angle α (rad)		
	Situation 1	Situation 2	Situation 3
Case 5	1.399	1.383	1.120
Case 6	2.354	1.644	1.523

a dynamic model established using a Newtonian approach. Next, a safety metric of avoiding tangling with a tensioned tether was designed to analyse the tangling risk of a tethered system. Based on that, several numerical cases were established and simulated. As shown in the simulation results, with the increase of attachment point bias, the amplitude of the oscillation of debris relative to the tether is significantly increased and the safe range is reduced, that is, a higher risk of tangling exists when there is a greater bias of capture, especially with the existence of a greater initial angular momentum. Moreover, the configuration with attachment point bias can be more dangerous in regard to tangling and more easily occurs in actual operation compared with the initial misalignment of the relative position and attitude between the space tug and target. In summary, a large attachment point bias, as in the case with appendages captured, should be rigorously avoided, and the attitude of debris should be taken into consideration as well, especially in a de-orbiting mission of large spinning debris. Furthermore, the method of suppressing dangerous oscillations of debris relative to the tether caused by attachment point bias should be explored in future work.

Acknowledgments

This research is supported by National Natural Science Foundation of China (51375034, 61327809) and Natural Science Foundation of Beijing (4172008).

References

[1] J.C. Liou, N.L. Johnson, N.M. Hill, Controlling the growth of future LEO debris populations with active debris removal, Acta Astronaut. 66 (5–6) (2010) 648–653.
[2] K.T. Nock, K.M. Aaron, D. Mcknight, Removing orbital debris with less risk, J. Spacecr. Rockets 50 (2) (2015) 365–379.
[3] Z. Chu, Y. Ma, Y. Hou, F. Wang, Inertial parameter identification using contact force information for an unknown object captured by a space manipulator, Acta Astronaut. 131 (2017) 69–82.
[4] R.L. Forward, R.P. Hoyt, C.W. Uphoff, Terminator Tether™: a spacecraft deorbit device, J. Spacecr. Rockets 37 (2) (2000) 187–196.
[5] M.P. Cartmell, D.J. Mckenzie, A review of space tether research, Prog. Aerosp. Sci. 44 (1) (2008) 1–21.
[6] V. Braun, A. Lüpken, S. Flegel, et al., Active debris removal of multiple priority targets, Adv. Space Res. 51 (9) (2013) 1638–1648.
[7] J.C. Liou, N.L. Johnson, A sensitivity study of the effectiveness of active debris removal in LEO, Acta Astronaut. 64 (2–3) (2009) 236–243.
[8] L.T. Deluca, F. Bernelli, F. Maggi, et al., Active space debris removal by hybrid engine module, In: 63rd International Astronautical Congress, Naples, Italy, 2012.
[9] J. Liu, N. Cui, F. Shen, et al., Dynamics of robotic geostationary orbit restorer system during deorbiting, IEEE Aerosp. Electron. Syst. Mag. 29 (11) (2014) 36–42.
[10] Robotic Geostationary Orbit Restorer (ROGER) Phase a Final Report, 2003. ESA Contract No.: 15706/01/NL/WK.
[11] Z. Meng, B. Wang, P. Huang, A space tethered towing method using tension and platform thrusts, Adv. Space Res. 59 (2) (2017) 656–669.
[12] G. Zhao, L. Sun, H. Huang, Thrust control of tethered satellite with a short constant tether in orbital maneuvering, Proc. Inst. Mech. Eng. Part G J. Aerosp. Eng. 228 (14) (2014) 2569–2586.
[13] M. Sabatini, P. Gasbarri, G.B. Palmerini, Elastic issues and vibration reduction in a tethered deorbiting mission, Adv. Space Res. 57 (9) (2016) 1951–1964.
[14] R. Zhong, Z.H. Zhu, Long term dynamics and optimal control of nano-satellite deorbit using a short electrodynamic tether, Adv. Space Res. 52 (8) (2013) 1530–1544.
[15] P. Huang, D. Wang, Z. Meng, F. Zhang, Z. Liu, Impact dynamic modeling and adaptive target capturing control for tethered space robots with uncertainties, IEEE/ASME Trans. Mechatron. 21 (5) (2016) 2260–2271.
[16] P. Huang, D. Wang, Z. Meng, F. Zhang, J. Guo, Adaptive postcapture backstepping control for tumbling tethered space robot–target combination, J. Guid. Control Dyn. 39 (1) (2016) 1–7.
[17] P. Huang, D. Wang, Z. Meng, F. Zhang, Z. Liu, Adaptive control for space debris removal with uncertain kinematics, dynamics and states, Acta Astronaut. 128 (2016) 416–430.
[18] P. Huang, M. Wang, Z. Meng, F. Zhang, Z. Liu, Attitude takeover control for post-capture of target spacecraft using space robot, Aerosp. Sci. Technol. 51 (2016) 171–180.
[19] P. Huang, D. Wang, Z. Meng, F. Zhang, Z. Liu, Postcapture robust nonlinear control for tethered space robot with constraints on actuator and velocity of space tether, Int. J. Robust Nonlinear Control (2016), http://dx.doi.org/10.1002/rnc.3712.
[20] V. Aslanov, V. Yudintsev, Dynamics of large debris connected to space tug by a tether, J. Guid. Control Dyn. 36 (36) (2013) 1654–1660.
[21] V. Aslanov, V. Yudintsev, Dynamics, analytical solutions and choice of parameters for towed space debris with flexible appendages, Adv. Space Res. 55 (2) (2015) 660–667.
[22] V. Aslanov, V. Yudintsev, Dynamics of large space debris removal using tethered space tug, Acta Astronaut. 91 (10) (2013) 149–156.
[23] K. Hovell, S. Ulrich, Attitude stabilization of an uncooperative spacecraft in an orbital environment using visco-elastic tethers, In: AIAA Guidance, Navigation, and Control Conference, San Diego, California, USA, 2016.
[24] A. Kheyfits, The theorem of cosines for pyramids,, Coll. Math. J. 35 (5) (2004) 385.